Stability of $(Ni_{1-x}Li_x)(Li_{1-y}Ni_y)O_2$ Ordered Solid Solution

V. Massarotti, D. Capsoni, and M. Bini

Department of Physical Chemistry and CSTE-CNR, Viale Taramelli,
University of Pavia, I-27100 Pavia

Z. Naturforsch. **50a** 155–168 (1995); received November 21, 1994

The stability of ordered solid solutions (OSS) with $LiNiO_2$ structure has been studied in a wide range of the lithium cationic fraction ($0.22 < x_t < 0.42$). The OSS is obtained from the reactive system NiO/Li_2CO_3 at 800 °C starting with high nominal lithium content ($x_t = 0.5$). By analysis of the decrease of x_t observed after annealing, during which evaporation and a contact reaction occurs, structure-composition relationships can be obtained.

The transformation of the ordered phase, due to a cation exchange process, is observed for $x_t \leq 0.31$ by accurate X-Ray powder pattern analysis (Rietveld method). By increasing the annealing time (decreasing lithium content), the data can be explained on the basis of progressive formation of the simple solid solution (SSS) with only one cation site and halved c axis value. The variations of structural parameters during the transformation are compared with those reported in the literature. The coherence domains of the OSS become smaller and the phase percentage decreases, while the SSS percentage increases. The rate of such a process can be well described on the basis of a two dimensional diffusion mechanism.

Key words: Lithium Nickel Oxides, Solid state reaction, Solid solution, Order-Disorder Transformation.

1. Introduction

Two main kinds of solid solutions have been studied in the system NiO/Li_2O for what concerns both their preparation and the electrical, magnetic and structural properties. $Li_xNi_{1-x}O$ is a substitutional solid solution (SSS), whose "NaCl-related" structure [1–5] has a unique cationic site and derives from NiO by cation substitution. The cubic cell (Space Group: Fm3m) can be rhombohedrally distorted (S.G.: R-3m) depending on composition. The SSS's are typical semiconductors and are widely used in the preparation of devices for electrochemical cells, e.g. ceramic electrodes for Molten Carbonate Fuel Cells (MCFC) [6, 7].

Another type of the general formula $(Ni_{1-x}Li_x)(Li_{1-y}Ni_y)O_2$ derives from the layered $LiNiO_2$ compound and can be defined as ordered solid solution (OSS) because of the preferred occupation of the two sites by different cations. Several $LiMO_2$ type compounds (M = V, Cr, Co, Ni) have recently been studied for their interest in ionic exchange and intercalation/de-intercalation processes. These compounds find applications both in the preparation of electrodes for lithium batteries [4, 8–14] and in the design of oxidation selective catalysts [15, 16]. Their structure is characterized by S.G. R-3m. The hexagonal cell is similar, but with a double c parameter with respect to the NiO related rhombohedral SSS. The oxygen ions form cubic-close-packed layers and the octahedral interstices between couples of adjacent oxygen planes contain the cations, M and Li, on alternate planes. Compounds having the same structure, but with more or less large deviation from stoichiometry, have been obtained both by solid state synthesis [11–13, 17] and by de-lithiation [18–20].

The thermal stability of the SSS was studied in a large composition range [5] using the reactive system Ni/Li_2CO_3. It was observed that the cation vacancy concentration increases with increasing lithium content and the temperature of annealing. In [21] the homogeneity of the solid solution was investigated by refining structural and profile parameters from X-ray data. The appearance of broad and asymmetrical diffraction peaks in dependence on the annealing time at 800 °C (while the Li content decreases) was explained by the presence of solid solutions of different composition and therefore with different values of the lattice parameters.

Crystallographic and magnetic properties of the phases present in the solid solution $Li_xNi_{1-x}O$ ($0 < x < 0.65$) were studied by Goodenough et al. [1]

Reprint requests to Prof. V. Massarotti.

0932-0784 / 95 / 0200-0155 $ 06.00 © – Verlag der Zeitschrift für Naturforschung, D-72027 Tübingen

and by Bronger et al. [2]. They found that partial cationic ordering occurs for $x > 0.28$ and suggested that ordering of the cations occurs in the alternate 003 planes. Recently, X-Ray [4, 12, 13] and neutron [15] powder diffraction investigations gave a thorough description of structure-composition relationships, order parameter, order-disorder transition and short range order. Ordering of cations in "sandwich"-type clusters was also revealed by EPR of Ni^{3+} [22]. However, the kinetics of the OSS transformation as a function of thermal treatment has never been studied.

In the present work we have studied the structure-composition relationship while the total Li content x_t changes in the range $0.22 < x_t < 0.42$ as a consequence of consecutive annealings of the sample. The range $0.22 < x_t < 0.31$, for which previous observations [12, 13, 15] seemed to indicate that Li and Ni are nearly randomly distributed in the cation site of the NiO structure, is carefully investigated. The samples are obtained from the reactive system NiO/Li_2CO_3 after different annealing times at 800 °C, starting from high nominal lithium content ($x_t = 0.5$). Low lithium content samples are obtained after very long annealing. The decrease of lithium content in the OSS is due both to evaporation and slow reactive processes (with the quartz or alumina of the vessel surface), and the change of order in lithium nickel oxide can be observed as a function of time.

2. Experimental

2.1. Materials

Li_2CO_3 (Merck 5671) and NiO obtained by decomposition of $NiSO_4 \cdot 7H_2O$ (Carlo Erba R.P.) were used for preparing the starting mixtures with 0.5 nominal lithium cationic fraction. The nickel sulfate hydrate was decomposed by heating the powder (heating rate 5°/min) up to 830 °C, holding at this temperature for 24 h and further annealing two times for 8 h at the same temperature. After each annealing the sample was ground in an agate mortar and tested for the presence of nickel sulfate by X-ray diffraction. After the treatment no sign of sulfate phase was revealed and the NiO particle size (approximately 0.1–0.2 μm) was determined by SEM observations.

2.2. Sample Preparation

The solid solutions studied in the present work were prepared starting from the reactive system NiO/Li_2CO_3. The reagents (0.5 lithium cationic fraction) were intimately mixed by grinding in an agate mortar and then heated at 5 °C/min up to 800 °C. An isothermal step at this temperature was held for the proper annealing time. The reactive process was performed in alumina and in quartz boats, both in bulk quantity and as low mass samples (in a thermogravimetric [TG] cell).

2.3. Apparatus and Procedures

Diffraction data were obtained by a Philips PW 1710 powder diffractometer equipped with a Philips PW 1050 vertical goniometer. Use was made of the Cu$K\alpha$ radiation ($K\alpha_1 = 1.5406$ Å; $K\alpha_2 = 1.5443$ Å) obtained by means of a graphite monochromator. Patterns were collected in the angular range $15° < 2\theta < 150°$ in step scan mode (step width: 0.03°; counting time: 1 s). Measurements were performed both on standard samples in an aluminum slide sample holder and on "thin samples" prepared by dispersing the powder (usually prepared in a TG cell) between two polyethylene films as described in [21, 23].

The thermal treatment of samples in the thermogravimetric cell was performed with a DuPont 1090 Thermal Analysis System equipped with a DuPont 951 Thermogravimetric Analyzer.

SEM micrographs were collected by a Cambridge Stereoscan 200 scanning electron microscope on gold sputtered samples (gold thickness about 150 Å).

Use was made of atomic absorption spectrometry to determine Li and Ni content of the samples.

Structural and profile parameters were obtained by the Rietveld refinement procedure [24]. The refinement was performed with the program DBW3.2S [25], to which reference should be made also for the meaning of the discrepancy factors (R_p, R_{wp}, R_B and GoF). The Rietveld method uses least squares procedures to minimize the residual

$$M = \sum w_i (y_{o,i} - y_{c,i})^2, \tag{1}$$

where $y_{o,i}$ represents the observed intensities collected at each point of the pattern; w_i is the statistical weight of each observation, in the following assumed as $w_i = 1/y_{o,i}$. The total intensity $y_{c,i}$ is calculated at point i for the general case of multiphase systems [26]:

$$y_{c,i} = \sum K_p \sum m_{h,p} L_{h,p} |F_{h,p}|^2 G_{h,p,i} A_{h,p,i} + y_{b,i}, \tag{2}$$

where K_p is the scale factor, $m_{h,p}$ the multiplicity of the reflection, $L_{h,p}$ the Lorentz-polarization factor, $F_{h,p}$

the structure factor, $G_{h,p,i}$ the peak profile function (a parametrized pseudo-Voigt function [27] is used), $A_{h,p,i}$ the peak asymmetry function, and $y_{b,i}$ the background intensity contribution. The double summation in (2) makes possible to take into account all the h reflection contributions of each p phase.

The fit between the observed patterns and the calculated ones was obtained on the basis of the following models:

i) SSS NiO type – Simple c axis hexagonal cell (R-3m).

$a \cong 2.91$ Å, $c \cong 7.13$ Å,

cationic site 0, 0, 0, anionic site 0, 0, 1/2.

ii) OSS $LiNiO_2$ type – Double c axis hexagonal cell (R-3m).

$a \cong 2.91$ Å, $c \cong 14.26$ Å,

cationic sites: 0, 0, 0 (type 3 a),
0, 0, 1/2 (type 3 b),

anionic site: 0, 0, z ($z \cong 1/4$).

The initial values for the lattice parameters were obtained by least squares fit from peak positions deduced from the indexed diffraction patterns. During the Rietveld refinement the lattice parameters were furtherly varied according to the procedure described in [21, 23]. The isotropic thermal parameters for the oxygen site and for the cationic sites were always varied independently. For each cationic site the sum of the atomic occupancy factors was constrained to unity. The values of the atomic scattering factors for Li^+ and Ni^{2+}, and for O^{2-}, reported in [28] and [29], respectively, were always used in the Rietveld refinements.

3. Results

The diffraction patterns of the samples show the lines expected for the layered $LiNiO_2$ structure [1, 2] even if the intensity of some lines (e.g. 003 and 101) changes remarkably as a function of time. For the most complete data set (samples annealed in a quartz boat) it can be seen that the intensity of such lines, that are typical of the presence of cationic ordering, increases at the beginning of the annealing (Fig. 1 a) and decreases after prolonged treatments (Figure 1 b). For very long annealing the same reflections almost disappear, although not completely (Figure 2). It was observed that, after annealing, the internal quartz wall was covered by a compact layer of lithium silicate, Li_4SiO_4. The same phase was found in traces in the samples, especially after long treatment. So, in this reacting system the loss of lithium from the $LiNiO_2$ structure can be due to both volatilization and reaction.

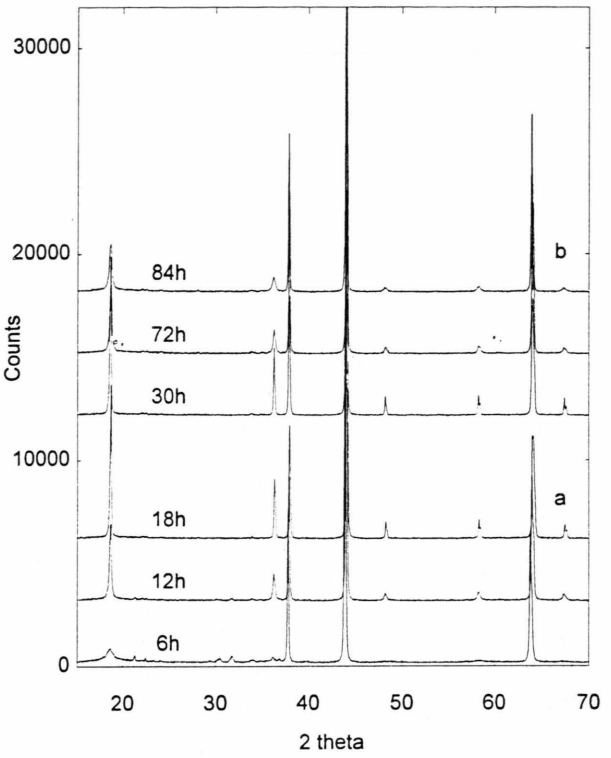

Fig. 1. Variation of the diffraction profile with the annealing time in a quartz boat: The OSS peak intensity increases with time at the beginning (a) and decreases with time after longer annealing (b).

On the contrary, for samples annealed in alumina (e.g. TG data set), only a decrease of superstructure reflections, such as 003 and 101, is observed as a function of time (Figure 3). The reaction between the reagents and the alumina wall was negligible, and no traces of aluminates were observed in the samples. The results of the structural analysis of the samples annealed in alumina and quartz boats are given in Table 1 and Table 2, respectively. For each data set are given: annealing time, t; profile discrepancy factor, R_p; weighted discrepancy factor, R_{wp}; goodness of fit, GoF; lattice parameters, a, c; hexagonal cell volume, V; rhombohedral distortion, $(c/a)/2\sqrt{6}$; Li occupancy

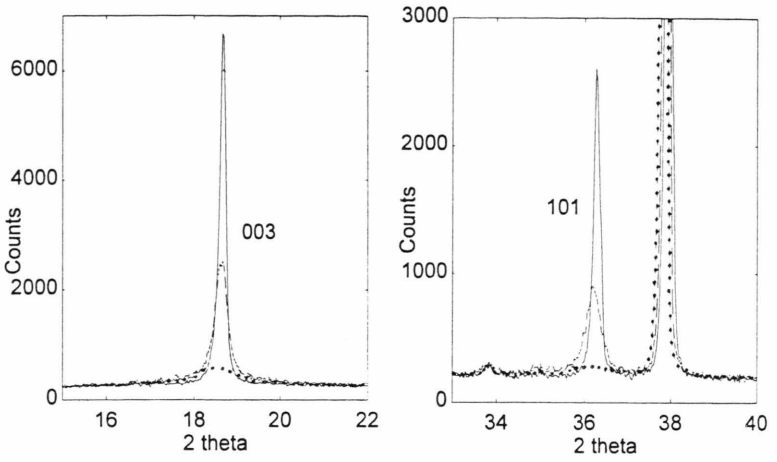

Fig. 2. Intensity variation with annealing time of 003 and 101 reflections of the OSS phase. The comparison is made among samples annealed 48 h (solid line), 84 h (dashed line) and 134 h (dotted line). Traces of Li_4SiO_4 phase are observed at $2\theta(°) \cong 34$.

of 3a and 3b sites; total lithium cationic fraction, x_t; generalized Bragg and Williams long range order parameter, S and oxygen z coordinate. In addition, the experimental values of full width at half maximum (FWHM) for the 003 peak, H_{003}, are reported.

Refinements were performed excluding the 003 reflection, whose calculated profile was not in satisfactory agreement with the experimental one because of strong asymmetry of the latter. Moreover, in some cases ($x_t < 0.31$ samples) the calculated FWHM for the 003 peak resulted sensibly underestimated. In Tables 1 and 2, in addition, are also reported R_{wp} and GoF values obtained by refining the complete data set (003 reflection included). For the samples annealed in

Table 1. Results of powder diffraction analysis of samples annealed in alumina (oven and TG-cell). Rietveld refinement has been performed according to the OSS model (see text).

	Oven			TG cell			
t/h	0	15	30	6	12	24	36
R_p	6.46	5.83	6.06	6.55	6.62	7.32	6.69
R_{wp}	8.26	7.64	7.83	8.51	9.53	9.16	8.39
GoF	1.26	1.15	1.20	1.17	1.35	1.21	1.24
R_{wp}	10.37	10.89	11.05	12.23	11.75	11.23	10.33
GoF	1.64	1.70	1.75	1.77	1.73	1.53	1.57
(003) included							
a/Å	2.89440 (8)	2.88977 (5)	2.89302 (4)	2.88742 (4)	2.88902 (6)	2.89340 (5)	2.89483 (6)
c/Å	14.23376 (58)	14.22887 (30)	14.23593 (28)	14.21408 (25)	14.22015 (36)	14.23014 (32)	14.23237 (36)
V/Å^3	103.268	102.903	103.186	102.629	102.787	103.171	103.289
$(c/a)/2\sqrt{6}$	1.003820	1.005082	1.004451	1.004854	1.004727	1.003911	1.003572
a site: $x_{Li,a}$	0.000	0.000	0.000	0.000	0.000	0.000	0.000
$x_{Ni,a}$	1.000	1.000	1.000	1.000	1.000	1.000	1.000
b site: $x_{Li,b}$	0.776 (4)	0.826 (3)	0.777 (3)	0.843 (2)	0.815 (4)	0.745 (5)	0.728 (4)
$x_{Ni,b}$	0.226 (4)	0.174 (3)	0.223 (3)	0.157 (2)	0.184 (4)	0.225 (5)	0.272 (4)
x_t [a]	0.388 (4)	0.413 (3)	0.389 (3)	0.422 (2)	0.408 (4)	0.373 (4)	0.364 (4)
x_{chem}	–	–	0.395 (5)	–	–	–	–
x_{TG}	–	–	–	$\leq$0.480 (7)	$\leq$0.450 (7)	0.378 (4)	0.357 (4)
S [b]	0.776 (4)	0.826 (3)	0.777 (3)	0.843 (2)	0.815 (4)	0.745 (5)	0.728 (4)
z	0.2578 (2)	0.2576 (2)	0.2573 (2)	0.2575 (2)	0.2576 (2)	0.2566 (3)	0.2565 (2)
H_{003}/degrees	0.176	0.158	0.141	0.135	0.137	0.134	0.134

[a] $x_t = (x_{Li,a} + x_{Li,b})/2$; [b] $S = x_{Li,b} - x_{Li,a}$.

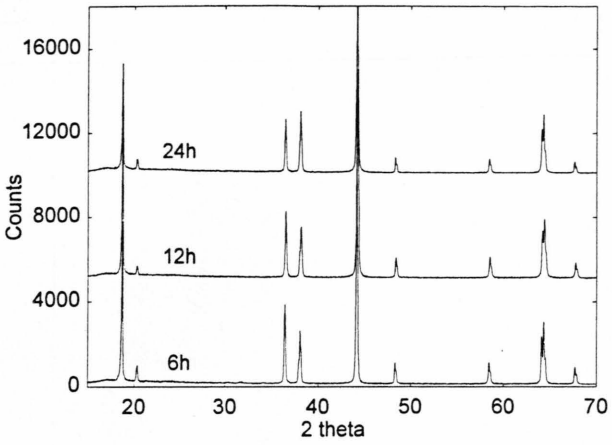

Fig. 3. Variation with time of the OSS peak intensity for samples annealed in alumina (TG cell). The peak appearing at $2\theta(°) \cong 20$ is due to the polyethylene film used for thin samples.

alumina (in oven or in TG cell) the fits are comparable for all data sets (Table 1). The observed, calculated and difference plots for the first data set of Table 1 are reported in Fig. 4, as an example.

The composition of the solid solutions (x_t) can be obtained from the occupancy values after Rietveld refinement. The sample composition is also obtained both by elemental analysis for Li and Ni, using atomic absorption (x_{chem}), and by analyzing thermogravimetric mass change data (x_{TG}) for comparison. The results are reported in Tables 1 and 2 and show fairly good agreement. TG measurements give the additional information that after 6 h annealing at least 4% Li_2CO_3 is still present. Because of the complex influence exerted on a mass change by Li_2CO_3 decomposition and Li_2O dissolution and volatilization, it is impossible to determine the amounts of the different contributions. However the upper limit of lithium content can

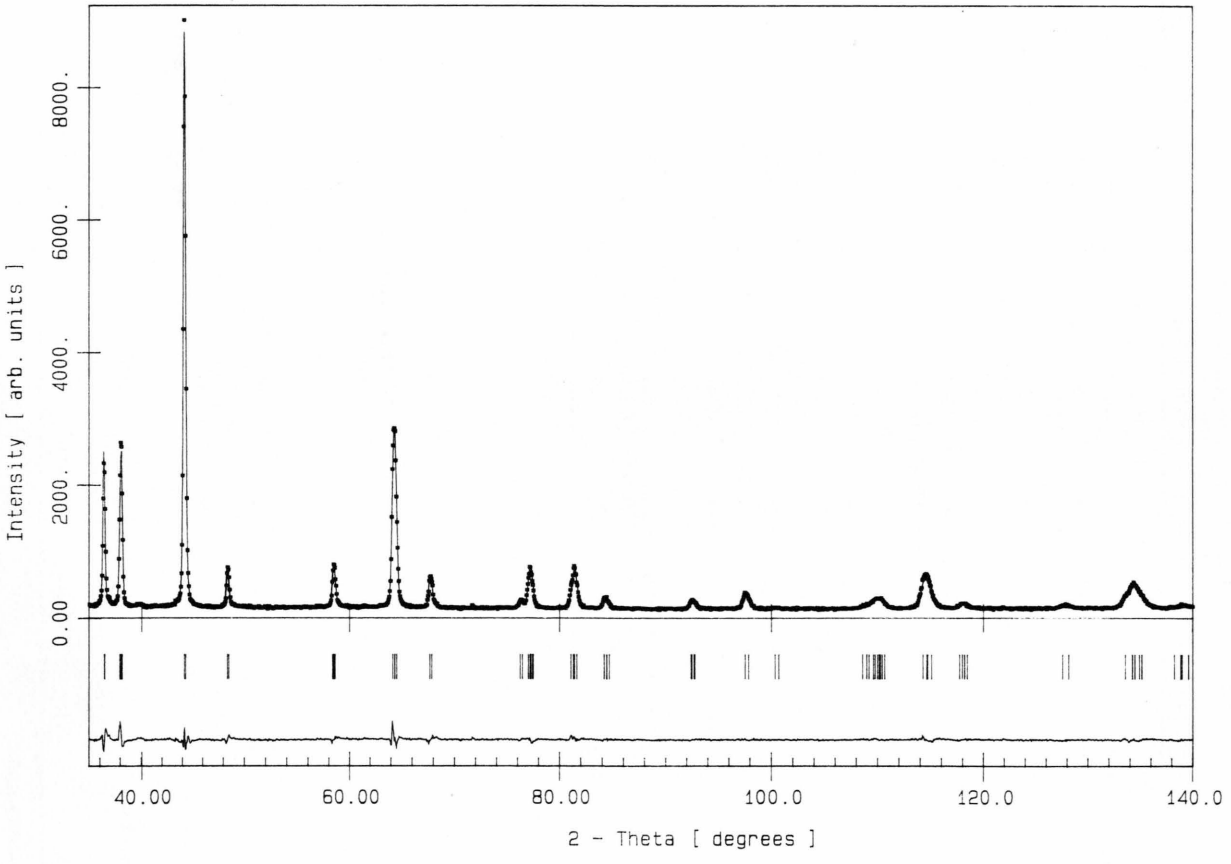

Fig. 4. Comparison between observed (squares) and calculated (solid line) pattern after Rietveld profile based on the OSS model for a sample not annealed at 800 °C. In the lower part the difference is plotted.

Table 2. Results of powder diffraction analysis of samples annealed in quartz. Rietveld refinement has been performed according to the OSS model (see text).

t/h	6	12	18	24	30	36	48	72	84	96	110	134
R_p	6.59	6.88	6.48	6.47	6.42	6.56	6.50	7.80	8.19	7.62	8.01	7.26
R_{wp}	8.78	9.26	8.19	8.15	8.13	8.23	8.34	10.36	10.88	10.27	10.45	9.31
GoF	1.45	1.50	1.33	1.34	1.34	1.37	1.36	1.70	1.78	1.66	1.66	1.49
R_{wp}	11.56	12.61	12.17	11.48	11.28	11.13	11.60	14.41	14.84	14.29	14.17	11.64
GoF	1.93	2.08	2.03	1.94	1.91	1.90	1.94	2.41	2.47	2.35	2.29	1.88
003 included												
a/Å	2.91123(30)	2.90580(8)	2.90136(3)	2.90067(3)	2.90115(2)	2.90162(2)	2.90380(3)	2.90700(7)	2.90762(7)	2.90826(14)	2.90921(16)	2.91255(26)
c/Å	14.26426(298)	14.24554(75)	14.24713(23)	14.24616(17)	14.24658(17)	14.24706(17)	14.25040(22)	14.24763(66)	14.24980(74)	14.24809(142)	14.25412(154)	14.26979(266)
V/Å^3	104.700	104.170	103.863	103.807	103.844	103.881	104.062	104.271	104.331	104.365	104.477	104.832
$(c/a)/2\sqrt{6}$	1.000155	1.000709	1.002352	1.002522	1.002386	1.002257	1.001739	1.000442	1.000381	1.000041	1.000138	1.000089
a site: $x_{Li,a}$	0.103(8)	0.029(7)	0.000	0.000	0.000	0.000	0.000	0.048(7)	0.076(8)	0.115(7)	0.133(8)	0.148(10)
$x_{Ni,a}$	0.897(8)	0.971(7)	1.000	1.000	1.000	1.000	1.000	0.952(7)	0.924(8)	0.885(7)	0.867(8)	0.852(10)
b site: $x_{Li,b}$	0.399(7)	0.567(5)	0.672(2)	0.682(2)	0.666(2)	0.658(2)	0.622(4)	0.534(5)	0.475(6)	0.441(6)	0.401(6)	0.305(10)
$x_{Ni,b}$	0.601(7)	0.433(5)	0.328(2)	0.318(2)	0.334(2)	0.342(2)	0.378(4)	0.466(5)	0.525(6)	0.559(6)	0.599(6)	0.695(10)
x_t	0.251(8)	0.298(6)	0.336(2)	0.341(2)	0.333(2)	0.329(2)	0.311(4)	0.291(6)	0.276(7)	0.278(7)	0.267(7)	0.227(10)
x_{chem}	–	–	–	–	0.345(5)	–	–	–	–	–	–	0.240(1)
S	0.296(15)	0.538(12)	0.672(4)	0.682(4)	0.666(4)	0.658(2)	0.622(8)	0.486(12)	0.399(14)	0.326(13)	0.268(14)	0.157(20)
z	0.2563(6)	0.2559(3)	0.2562(2)	0.2566(2)	0.2561(2)	0.2562(2)	0.2557(2)	0.2552(3)	0.2548(4)	0.2547(4)	0.2541(5)	0.2552(8)
H_{003}/degrees	0.988	0.270	0.151	0.149	0.163	0.153	0.164	0.284	0.372	0.469	0.635	1.434

Table 3. Results of SRO and LRO analysis for the 003 peak region of samples annealed in quartz.

t/h	6	12	18	24	30	36	48	72	84	96	110	134
x_t	0.251(8)	0.298(6)	0.336(2)	0.341(2)	0.333(2)	0.329(2)	0.311(4)	0.291(6)	0.296(7)	0.278(7)	0.267(7)	0.227(10)
$H_{SRO,003}$/degrees	5.729	2.375	–	–	–	–	–	3.56	4.20	4.0	4.0	4.0
$I_{SRO,003}$*	973(206)	65(24)	–	–	–	–	–	79(31)	269(38)	500(50)	435(42)	400(50)
L_{SRO}/Å	14(1)	36(2)	–	–	–	–	–	23(2)	20(2)	21(2)	21(2)	21(2)
I_{SRO}/I_{003}	0.717(59)	0.066(24)	–	–	–	–	–	0.083(20)	0.261(20)	0.385(5)	0.441(30)	0.475(64)
I_{SRO}/I_{004}	0.090	0.024(9)	–	–	–	–	–	0.029(7)	0.084(6)	0.109(2)	0.108(7)	0.083(2)
H_{LRO}/degrees	0.738	0.221(4)	0.139(3)	0.121(3)	0.131(3)	0.126(3)	0.139(3)	0.238(4)	0.310(6)	0.655(19)	0.524(15)	1.48(9)
I_{LRO}*	385(23)	915(11)	1181(16)	1182(20)	1182(18)	1157(17)	1030(12)	875(10)	761(10)	820(20)	551(14)	442(21)
L_{LRO}/Å	127(8)	700(30)	2440(400)	5300(900)	3200(400)	4000(500)	2440(400)	610(20)	395(12)	147(5)	193(7)	59(5)

* Arbitrary units.

be evaluated ($x_{TG} \leq 0.48$). The same contributions are present after 12 h annealing and the upper limit of lithium content ($x_{TG} \leq 0.45$) is still far from the structural result ($x_t = 0.41$). After 24 and 36 h annealing the TG mass change can be interpreted on the basis of the prevalent mechanism of solid solution decomposition and lithium oxide volatilization. The relevant x_{TG} values are in good agreement with the x_t ones.

4. Discussion

4.1. Cationic Ordering from Refinement Results

For compounds of the general formula $(Ni_{1-x}Li_x)_{(3a)}(Li_{1-y}Ni_y)_{(3b)}O_2$ the first evidence of changes in site occupancies can be found in changes in X-ray intensities. Morales et al. [4] showed that these changes are specially evident if the intensity ratio I_{003}/I_{104} is observed. The 003 reflection is only typical for the ordered double cell structure (OSS), while the reflection 104 of the same phase is substituted by the 102 one in the hexagonal cell with halved c axis and a unique cationic site (SSS) or by the 400 one in the other limiting cubic NaCl-related structure. The plot of Fig. 5a shows the dependence on annealing time of the I_{003}/I_{104} ratio. For the most complete data set of Table 2 the highest values of intensity ratio are obtained for samples annealed for 18 to 48 h. Low mass samples obtained in the TG cell (annealed in alumina) give a quite different trend of I_{003}/I_{104} vs. time. In particular the ratio is much higher for short annealing times, decreases monotonously with increasing time and after 36 h is lower than that pertinent for 96 h in quartz. A more comparable trend among the different data sets can be obtained by plotting the Li occupancy obtained for the two cationic sites, as shown in Fig. 5b, where the order parameter S is also reported. The maximum degree of order is observed in a limited time range (approximately 15 to 50 h), which is characterized by the presence of Li on 3b cation sites only, with an occupancy factor ranging between 0.62 and 0.68. The occupancy factors are obtained without strong correlation between the same parameters and the isotropic thermal factors. S increases in the first time range (0–15 h), remains nearly constant in the second range (15–50 h), and decreases monotonically during the third range ($t > 72$ h), while the Li occupancy of 3a site increases. This trend describes the change of order in the compound $(Ni_{1-x}Li_x)_{(3a)}(Li_{1-y}Ni_y)_{(3b)}O_2$ while the total lithium content attains the maximum and then decreases below the critical value 0.31.

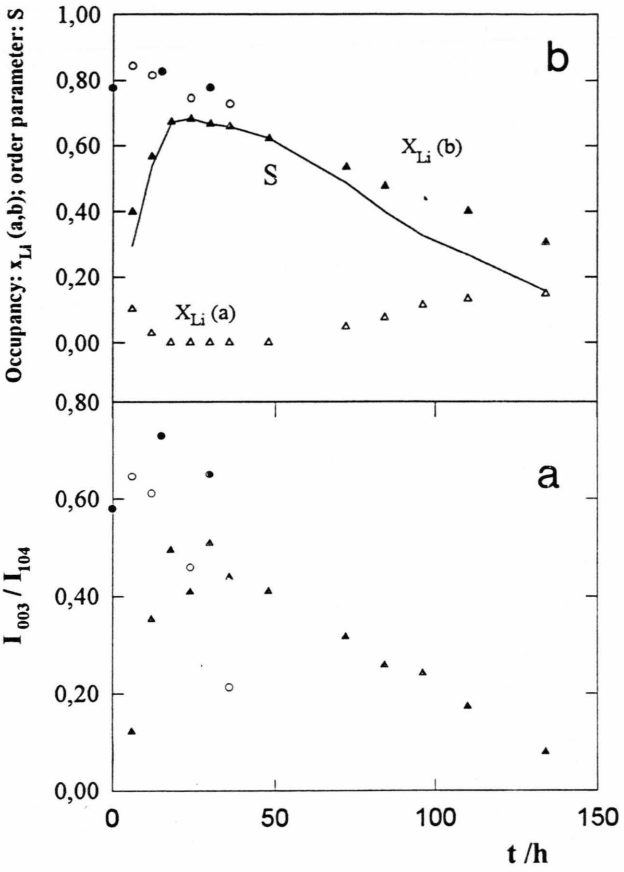

Fig. 5. Dependence on annealing time of: (a)I_{003}/I_{104} ratio for samples annealed in quartz (▲) and in alumina (oven: ●; TG: ○); (b) Li occupancy in 3b site (▲), in 3a site (△), order parameter S (solid line) defined as the difference of Li occupancy in the two sites (see Table 2).

For the other samples, obtained in alumina, both in oven and in the TG cell (Table 1), the refinement gives remarkably higher Li occupancies on 3b cation sites, and hence higher total Li content, than those obtained in quartz. This can be due to different reactivity of lithium oxide with the container wall. The process may occur during the entire annealing but shows its main influence in the beginning.

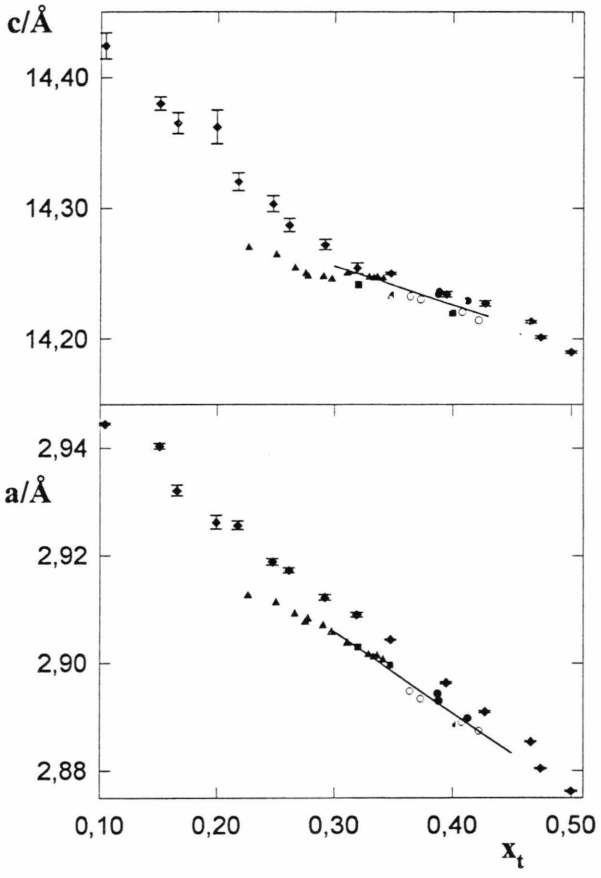

Fig. 6. Variation of hexagonal lattice parameters a and c with lithium content, x_t. Data from this work, obtained from samples annealed in quartz (▲) and in alumina (oven: ●; TG: ○), are compared with those of [12] (◆) and [15] (■).

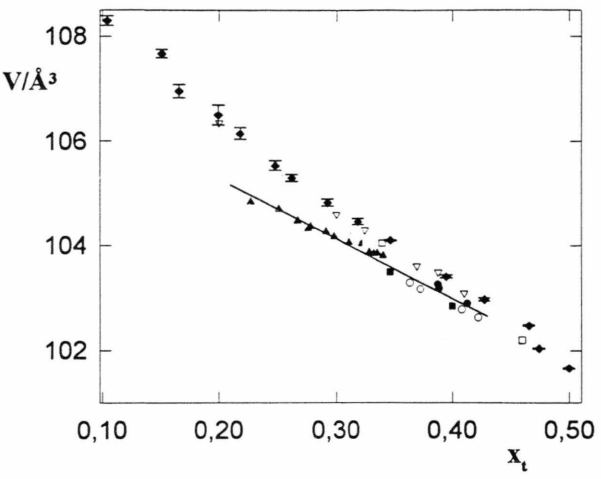

Fig. 7. Variation of hexagonal cell volume vs. Li content. Data from this work, obtained from samples annealed in quartz (▲) and in alumina (oven: ●; TG: ○), are compared with those of [1] (▽), [4] (□), [12] (◆) and [15] (■).

4.2. Lattice Parameters and Cell Volume

The lattice parameters determined by refinement (Tables 1, 2) show a smooth variation with Li content. A linear dependence of the a parameter is well observed for $0.31 < x_t < 0.42$: $a = 2.95113 - 0.15074\,x_t$. A plot of a vs. x_t is shown in Figure 6a. The a values pertinent to the region $x_t < 0.31$ (Table 2) are slightly lower than those deducible from the linear relation.

A plot of c vs. x_t is shown in Figure 6b. Also this parameter depends linearly on composition in the range $0.31 < x_t < 0.42$: $c = 14.34482 - 0.29702\,x_t$. Strong correlations and greater standard deviations are only observed for the a and c parameters of samples whose fits are less satisfactory ($x_t < 0.31$).

The correlation between lattice parameters is not expected to affect sensibly the linear dependence of the cell volume on the lithium content, at least for $x_t > 0.31$. The plot in Fig. 7 shows that the relation $V = 107.5390 - 11.3605\,x_t$ can be assumed in the entire range $0.22 < x_t < 0.42$ ($R = 0.990$). Values taken from the literature [1, 4, 12, 15] are also reported for comparison. The best agreement exists with the data of Pickering et al. Discrepancies in composition and/or in lattice parameters can be responsible for the observed discrepancies in the V values. Then, it can be observed that, for the same laboratory, the knowledge of the coefficients of the linear function of V vs. x_t might be helpful to determine the lithium content from the experimental values of the lattice parameters [11, 15]. Consequently it is not surprising that a systematic difference has been found by Pickering et al. [15] between their Li content values (obtained by chemical analysis) and those deduced by a known linear dependence V on x_t [1, 4] using their lattice parameters.

4.3. Rhombohedral Distortion

For the structure of the compound $(Ni_{1-x}Li_x)_{(3a)}(Li_{1-y}Ni_y)_{(3b)}O_2$ the rhombohedral distortion represents an important characteristic [1, 4, 12, 13, 15], which can be defined as the deviation of the ratio c/a with respect to the ideal cubic value $2\sqrt{6}$. The values obtained are reported in Tables 1 and 2. When expressed as percentage variation [1, 4, 15],

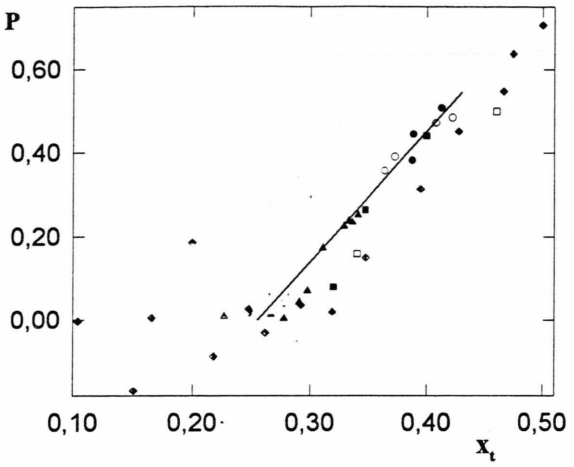

Fig. 8. Percentage variation of rhombohedral distortion (see text) vs. Li content. Data from this work, obtained from samples annealed in quartz (▲) and in alumina (oven: ●; TG: ○), are compared with those of [4] (□), [12] (◆) and [15] (■).

$P = 100\,[(c/a)/(2\sqrt{6}) - 1]$, a plot of P vs. x_t (Fig. 8), shows the decrease of P with decreasing x_t. Some scatter of data, comparatively larger than that observed for the V vs. x_t plot, can be due to the presence of correlation, low but negative, between a and c refined values. For samples annealed more than 72 h and for those annealed for a short time as well (i.e. samples with low Li content), a larger uncertainty in the P values must be expected. Anyway, the general smooth variation of P as a function of x_t is clearly observed and compared with other data previously reported in the literature [4, 12, 15]. As deduced by Li et al. [12] and by Pickering et al. [15], P should vanish at the limiting composition for the cubic-rhombohedral transition $x_t = 0.31$. However, considering the variation in the metal-oxygen bond length for the two cation sites [15], and from the observation of broad and diffuse superlattice reflections in a cubic low lithium content sample, it was suggested [12, 15] that some degree of order is still present for $x_t \leq 0.31$. The trend of our P values for low Li content shown in Fig. 8, together with the result of the linear extrapolation of our high Li content results, seem to confirm such a hypothesis. A change in the trend of P is indeed observable for $x_t \cong 0.31$.

For a better understanding of the behaviour of rhombohedral distortion of low lithium content samples it is necessary on one side to state the homogeneity degree of these samples, on the other side to explain why Rietveld profile refinements of their patterns give systematically less satisfactory fits than those obtained for samples with higher lithium content, annealed for 15 to 50 hours. It must be reminded that samples annealed for only a few hours (<15 h) can contain lithium carbonate impurity. However, the influence on the fit should be negligible and can be eliminated by excluding some limited angular regions. Samples obtained after very long annealing (> 50 h) can contain impurity due to contamination from the vessel material. Also in this case, the influence on the quality of the fit is negligible.

4.4. Transformation of the Ordered Solid Solution

A detailed comparison of the patterns for the three annealing ranges (refer to Fig. 5b and Table 2 for specifying the ranges) allows to point out some details of the results pertinent to the samples of the two extreme annealing conditions.

a) Samples Annealed for less than 15 h

Two sets of reflections can be observed (I and II). They are characterized by two distinct line widths, w_I and w_{II}, with $w_I > w_{II}$. Type I reflections are pertinent to an ordered structure cell, type II reflections are pertinent to a simple cell (with one cation site randomly occupied).

Line width and intensity of set I peaks depend on the annealing time: w_I decreases with increasing t, the intensity increases with t.

b) Samples Annealed for more than 50 h

Two sets of reflections can be observed as reported in a);

w_I increases with t, the intensity of set I peaks decreases with t.

As a result of Rietveld profile refinement on data obtained after extreme annealing conditions the line profile fitting is satisfactory for set II reflections only. Figure 9 shows, for the 84 h annealed sample, the FWHM obtained by Rietveld refinement as a function of the reflection angle together with the FWHM values for both type I and type II reflections obtained by individual profile fitting. It can be seen that the calculated trend agrees with the FWHM of set II peaks only. Taking into account the presence of short-range order scattering (SRO) [13], it is possible to explain in

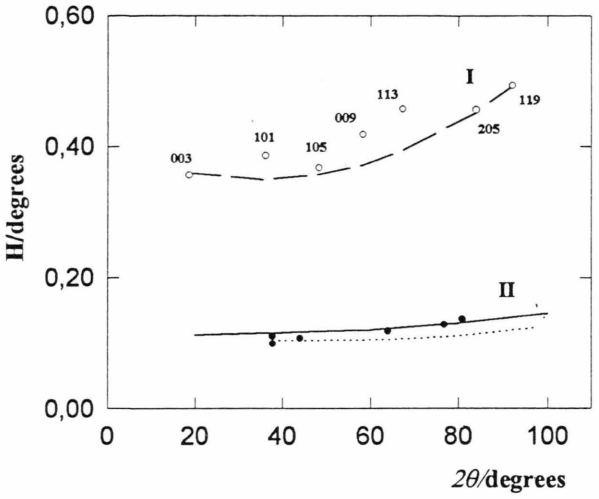

Fig. 9. FWHM values from individual profile fittings for type I (○) and II (●) reflections compared with the calculated FWHM angular dependence by single phase Rietveld refinement (OSS, solid line) and by the two-phase model (OSS, dashed line; SSS, dotted line).

part the considerable profile broadening observed for type I peaks, in particular for what concern their long tails. The results of peak profile fitting of 003 reflection, using two lorentzian profiles for SRO and long-range order (LRO) contributions, are reported in Table 3. The coherence length values for both SRO and LRO components are obtained by the Scherrer formula taking into account the instrumental broadening (equal to $0.106° 2\theta$). The lorentzian shape of profiles allows one to consider the simplified model of additivity of instrumental and sample (crystallite size) breadth components to give the observed line width [30]. For samples with $x_t < 0.31$, both SRO and LRO are present; no SRO contribution is observed in samples with $x_t > 0.31$. The SRO coherence length is nearly constant while the LRO coherence length decreases with decreasing lithium content. The intensity contributions of SRO scattering relative both to the total 003 and 104 integrated intensities increase with decreasing lithium content for $x_t < 0.31$. A different dependence of the SRO intensity on the lithium content is given in the literature [13]: we are quite confident that in our samples the inhomogeneous region can be limited to the range $x_t < 0.31$.

The above observations suggest the formation of a new ordered phase during the first range, where the lithium content increases, and the destruction of the same phase during the third range, due to Li content decrease and random solid solution formation. In both ranges the system should be considered a two phase system, and structural refinements should be undertaken using a suitable model. Recent evidence of two-phase system after higher temperature treatments ($T > 850\,°C$) and quenching [31] has been explained on the basis of $LiNiO_2$ decomposition and formation of partially disordered $Li_{1-x}Ni_{1+x}O_2$ and fully disordered $Li_xNi_{1-x}O$.

4.5. A Model for the Transformation

The gradual decrease of mean cationic order as the lithium content decreases can be described by considering the initial crystallite sizes to be nearly the same as L_{LRO}. During the annealing some crystallite boundary loses order after lithium loss and cation exchanges: nucleation of a new disordered phase starts with a local order parameter, S_D, much smaller than the mean crystallite order, S_O. At the same time antiphase domains can form whose presence would have relevant effects on the broadening of the superstructure reflections. However, because of the long annealing of the samples, an appreciable contribution of antiphase domains to the broadening should not be observed. Using a polycrystalline sample, made of a great amount of crystallites statistically oriented, a diffraction experiment shows a pattern equal to the sum of diffraction effects due to the lattices of the different phases. In the present system there are two phases differing in lithium content, degree of order, lattice parameters and crystallite size. The model adopted for the Rietveld profile refinement includes the following phases: I – OSS, as previously reported in 2.3, to describe the superstructure peaks whose integrated intensities particularly depend on the order parameter; II – SSS, to describe the most intense peaks of the patterns having pronounced overlapping with the fundamental reflection of the OSS phase.

Structural data pertinent to the two phases of the model can be obtained as follows. For each phase, lattice parameters, profile parameters, isotropic thermal factors, occupancy factors and structure factors are independently obtained by refinement. The percentages of the two phases are calculated from the scale factors of the phases according to the procedure of Hill and Howard [26]. Two phase refinement is performed using 10 structural parameters (6 and 4, respectively, for phase I and II), 14 profile parameters (4 gaussian, 2 lorentzian and 1 asymmetry, for each

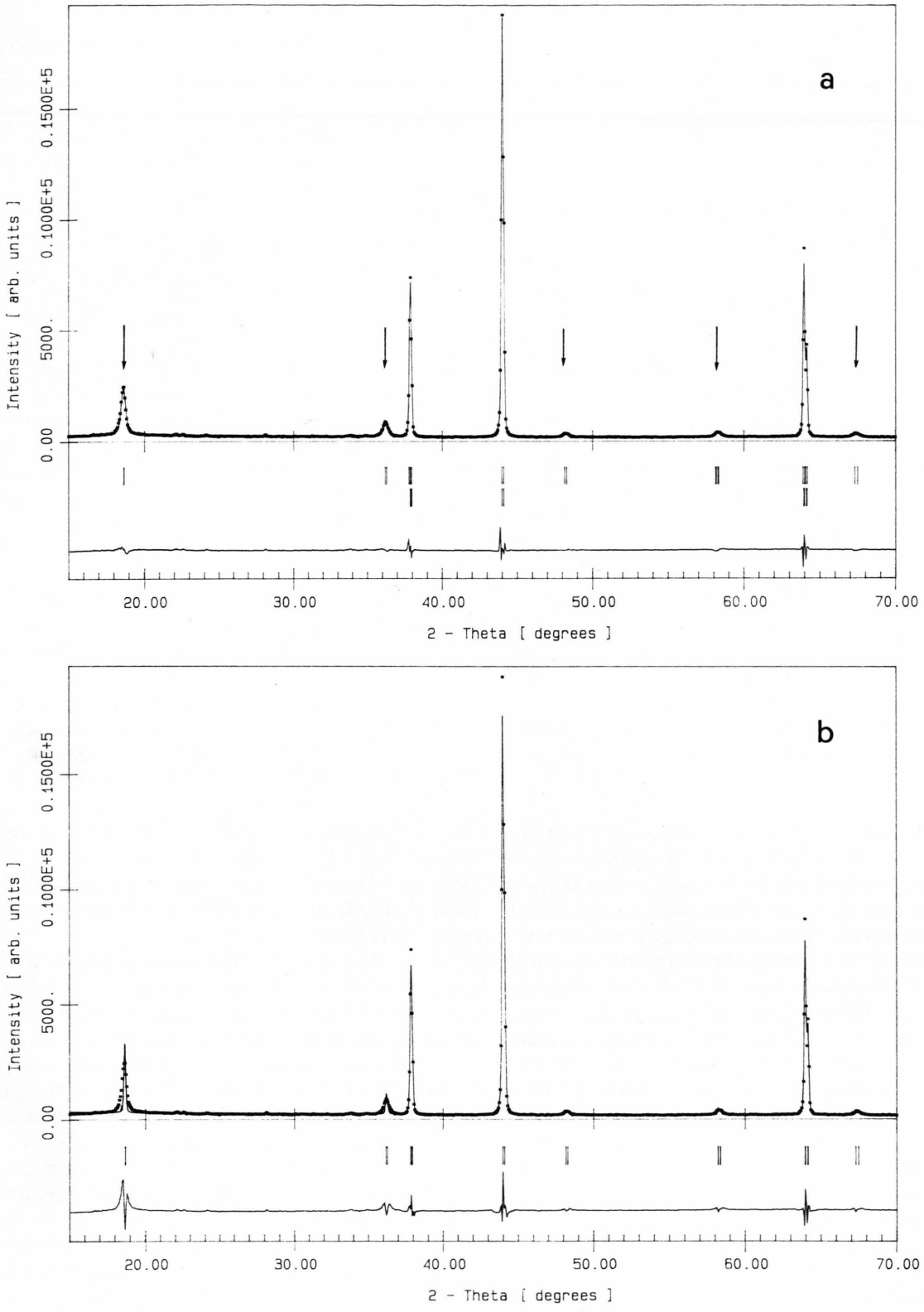

Fig. 10. Comparison between observed (squares) and calculated (continuous line) pattern after Rietveld profile refinement based on two-phase model (a) and single-phase model (b).

Table 4. Results of powder diffraction analysis of samples annealed in quartz. Rietveld refinement has been performed according to the two-phase model: OSS + SSS (see text).

t/h	6	12	72	84	96	110	134
R_p	7.33	8.35	7.39	7.73	7.46	7.84	7.21
R_{wp}	10.14	10.61	9.46	9.68	9.61	10.14	9.48
GoF (003 included)	1.69	1.75	1.57	1.61	1.57	1.63	1.52
OSS phase							
R_B	23.68	6.06	12.18	9.51	13.23	25.28	24.13
a/Å	2.9105	2.9037	2.9052	2.9065	2.9080	2.9091	2.9067
c/Å	14.2746	14.2674	14.2686	14.2704	14.2711	14.2599	14.2722
V/Å^3	104.720	104.179	104.300	104.402	104.515	104.512	104.429
$(c/a)/2\sqrt{6}$	1.0011	1.0030	1.0025	1.0022	1.0017	1.0006	1.0023
a site: $x_{Li,a}$	0.000	0.000	0.000	0.000	0.000	0.000	0.000
$x_{Ni,a}$	1.000	1.000	1.000	1.000	1.000	1.000	1.000
b site: $x_{Li,b}$	0.706(14)	0.682(4)	0.777(18)	0.864(22)	0.894(6)	0.818(49)	0.910
$x_{Ni,b}$	0.294(14)	0.318(4)	0.223(18)	0.136(22)	0.106(6)	0.182(49)	0.090
% OSS	20(1)	76(1)	41(2)	32(2)	25(2)	16(1)	10(1)
z	0.2670	0.2584(3)	0.2611(5)	0.2635(6)	0.2649(6)	0.2731(16)	0.2690
SSS phase							
R_B	2.08	3.80	2.59	2.38	1.82	2.55	1.99
a/Å	2.9114	2.9052	2.9069	2.9069	2.9075	2.9088	2.9124
c/Å	7.1314	7.1271	7.1234	7.1279	7.1277	7.1288	7.1357
V/Å^3	52.341	52.095	52.130	52.162	52.182	52.237	52.420
$(c/a)/\sqrt{6}$	1.0000	1.0015	1.0004	1.0010	1.0008	1.0005	1.0003
Li occupancy	0.241(7)	0.188(16)	0.280(8)	0.252(7)	0.261(6)	0.219(6)	0.221(6)
% SSS	80(2)	24(1)	55(3)	64(2)	71(2)	80(2)	86(2)

phase) and 4 to 6 global (background) parameters. Figure 9 shows, for the 84 h annealed sample, also the results of the FWHM fit for both set I and set II peaks after the two-phase refinement (dashed and dotted curves). Figure 10 shows the best agreement between observed and calculated patterns with the two-phase model (a) compared with that obtained with the mono-phase model (b), for the 84 h annealed sample. Only in the first case both the larger OSS peaks (indicated by arrows) and the narrower SSS peaks can be suitably explained. The two-phase model has been used for all the samples with $x_t < 0.31$. The results of the refinements are given in Table 4, where the mass percentages for the OSS and SSS phases are also reported.

The assumption of the two phase model allows us to deduce that:

– The mass percentage of ordered phase shows opposite variations in the first and third range. In the first one the OSS increases with time while the global Li content x_t increases and the Li occupancy on 3b site remains approximately constant. The first forming SSS has high lithium content, then in a few hours a large part of it transforms into the lithium richer OSS phase that remains in equilibrium with the lower Li content SSS phase.

– In the third range the OSS decreases with increasing time, while x_t decreases and the Li occupancy (on 3b site) remains nearly constant. After long annealing the OSS transforms slowly, while its Li content remains constant, into a SSS phase with lower Li content. The mean values $x_{Li(SSS)} = 0.24(4)$ and $x_{Li(OSS)} = 0.40(5)$ are obtained from the pertinent values reported in Table 4.

– From the mass percentages of the OSS and SSS reported in Table 4 the degree of transformation of the former into the latter,

$$\alpha = \%SSS/(\%SSS + \%OSS), \tag{3}$$

can be deduced as a function of time. Such a transformation follows a two-dimensional diffusion mecha-

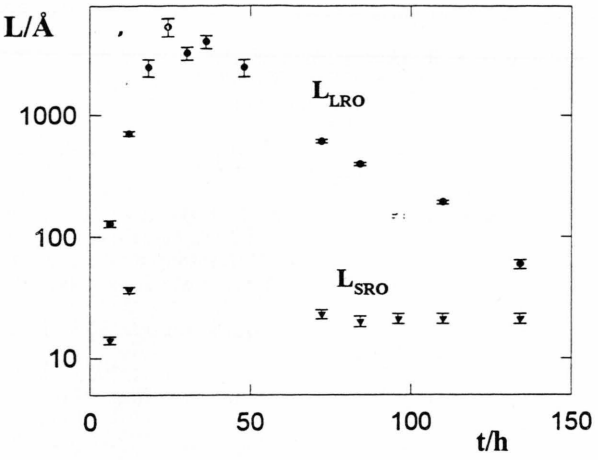

Fig. 11. LRO (●) and SRO (▼) coherence lengths, perpendicular to the 003 lattice planes, vs. annealing time.

nism. According to the equation

$$\alpha + (1 - \alpha)\ln(1 - \alpha) = k(t - t_0) \qquad (4)$$

the values $t_0 = 43$ h and $k = 7.47 \cdot 10^{-3}\ \mathrm{h}^{-1}$ are obtained.

– The lattice parameters and hence the cell volume and rhombohedral distortion of the two phases show a quite regular trend during the transformation occurring in the first and in the third annealing range. The most evident variations occur for the first and the last sample. In these cases the deviations can be due to the less significant OSS lattice parameters because of both the low contribution of the phase and the very remarkable broadening of its peaks.

– The variation in peak broadening as a function of annealing time, more evident in the third range, can be observed during the whole treatment. The measurement of the line broadening of the OSS peaks, particularly for the 003 reflection (Table 3) enables one to deduce the SRO and LRO coherence lengths. The plot of L_{LRO} vs. annealing time (Fig. 11) shows the rapid increase of the OSS coherence length in the first few hours of the annealing, followed by a stability range of the same phase, and then by a monotonic decrease in L values as the order disappears. This solid state transformation requires more than 100 h in the present conditions.

It can now be understood why the P values for samples with $x_t < 0.31$ in Fig. 8 cannot have the same significance as the other ones. In this composition range the parameter deduced from single phase structural refinement may be incorrect or misleading because of the presence of a second phase not included in the model.

5. Conclusions

Samples of the layered compound $Ni(Li_{1-y}Ni_y)O_2$ can be obtained in the reactive system NiO/Li_2CO_3 with initial Li cationic fraction $x_t = 0.50$ through annealing at 800 °C. After a sufficiently long annealing time, depending on the reaction conditions, the lithium content and order parameter gradually decrease because of evaporation and contact reactions. The transformation can take place when part of the system (boundary phase) contains less than a critical lithium cationic fraction (0.31): the ordered phase becomes unstable and forms the simple solid solution $Li_xNi_{1-x}O$. At the same time significant LRO and SRO effects are observed. The percentage of SSS increases and the OSS phase maintains its Li content while its percentage decreases. The rate of SSS formation can be well described on the basis of a diffusion mechanism by which the cation occupancy randomizes. So, the SSS, and OSS phases transform easily into one another, each of them at the proper lithium content, the driving force being the Li concentration and the direction of the gradient. The coexistence of the two-phases in the system makes the study of some properties in the composition range $0.20 < x_t < 0.31$ quite difficult. For this reason the results should be critically evaluated, particularly for samples subjected to long thermal treatment.

The kinetics of the transformation is now being studied and will be reported in a further paper.

Acknowledgement

This work has been supported by MURST 40% funds.

[1] J. B. Goodenough, D. G. Wickham, and W. J. Croft, J. Phys. Chem. Solids **5,** 107 (1958).
[2] V. W. Bronger, H. Bade, and W. Klemm, Z. Anorg. Allg. Chem. **333,** 188 (1964).
[3] C. J. Toussaint, J. Appl. Cryst. **4,** 293 (1971).
[4] J. Morales, C. Perez Vicente, and J. L. Tirado, Mater. Res. Bull. **25,** 623 (1990).
[5] A. Marini, V. Massarotti, V. Berbenni, D. Capsoni, R. Riccardi, E. Antolini, and B. Passalacqua, Solid State Ionics **45,** 143 (1991).
[6] J. R. Selman and T. D. Claar, eds., in: Molten Carbonate Fuel Cell Technology, Electrochem Soc., Pennington, NJ 1982.
[7] K. Kinoshita, F. R. Larnon, and E. J. Cairns, Fuel Cells, a Handbook (DOE/METC-88/6096), Chapter 4.
[8] L. D. Dyer, B. S. Borie, Jr., and G. P. Smith, J. Amer. Chem. Soc. **76,** 1499 (1954).
[9] T. A. Hewston and B. L. Chamberland, J. Phys. Chem. Solids **48,** 97 (1987).
[10] M. M. Thackeray, L. A. de Picciotto, W. I. F. David, P. G. Bruce, and J. B. Goodenough, J. Solid State Chem. **67,** 285 (1987).
[11] J. R. Dahn, U. Von Sacken, and C. A. Michal, Solid State Ionics **44,** 87 (1990).
[12] W. Li, J. N. Reimers, and J. R. Dahn, Phys. Rev. **B 46,** 3236 (1992).
[13] J. N. Reimers, W. Li, and J. R. Dahn, Phys. Rev. **B 47,** 8486 (1993).
[14] T. Ohzuku, A. Ueda, and M. Nagayama, J. Electrochem. Soc. **140 (7),** 1862 (1993).
[15] I. J. Pickering, J. T. Lewandowski, A. J. Jacobson, and J. A. Goldstone, Solid State Ionics **53–56,** 405 (1992).
[16] H. Hatano and K. Otsuka, JCS Faraday Trans. **I 85,** 199 (1989).
[17] M. G. S. R. Thomas, W. I. F. David, and J. B. Goodenough, Mater. Res. Bull. **20,** 1137 (1985).
[18] K. Vidiasagar and J. Gopalakrishnan, J. Solid State Chem. **42,** 217 (1982).
[19] L. A. de Picciotto, M. M. Thackeray, W. I. F. David, P. G. Bruce, and J. B. Goodenough, Mater. Res. Bull. **19,** 1497 (1984).
[20] K. Mizushima, P. C. Jones, P. J. Wiseman, and J. B. Goodenough, Mater. Res. Bull. **15,** 783 (1980).
[21] V. Berbenni, V. Massarotti, D. Capsoni, R. Riccardi, A. Marini, and E. Antolini, Solid State Ionics **48,** 101 (1991).
[22] R. Stoyanova, E. Zhecheva, and S. Angelov, Solid State Ionics **59,** 17 (1993).
[23] V. Massarotti, D. Capsoni, V. Berbenni, R. Riccardi, A. Marini, and E. Antolini, Z. Naturforsch. **46a,** 503 (1991).
[24] H. M. Rietveld, J. Appl. Cryst. **2,** 65 (1969).
[25] D. B. Wiles and R. A. Young, J. Appl. Cryst. **14,** 149 (1981).
[26] R. J. Hill and C. J. Howard, J. Appl. Cryst. **20,** 467 (1987).
[27] P. Thompson, D. E. Cox, and J. B. Hastings, J. Appl. Cryst. **20,** 79 (1987).
[28] International Tables for X-Ray Crystallography **Vol. IV,** Kynok Press, Birmingham 1974, pp. 99, 149.
[29] E. Hovestreydt, Acta Cryst. **A 39,** 268 (1983).
[30] H. P. Klug and L. E. Alexander, "X ray diffraction procedures", J. Wiley, New York 1974, Chapter 9.
[31] R. Kanno, H. Kubo, Y. Kavamoto, T. Kamiyama, F. Izumi, Y. Takeda, and M. Takano, J. Solid State Chem. **110,** 216 (1994).